WARSAW UNIVERSITY OF TECHNOLOGY Index 351733
FACULTY OF CIVIL ENGINEERING
COMMITTEE FOR CIVIL AND WATER ENGINEERING
POLISH ACADEMY OF SCIENCES ISSN 1230-2945
DOI: 10.24425/ace.2024.148930
ARCHIVES OF CIVIL ENGINEERING
Vol. LXX ISSUE 1 2024
pp. 589–604

Research paper

Study on failure modes and calculation method of the cast steel joint with branches in treelike structure

Feng Chen[1], Yun Sun[2], Shuxuan Sun[3], Da Song[4], Yangbing Liu[5]

Abstract: The treelike structure links members and transfers loads via its solitary cast steel joint with branches. Therefore, the joint's bearing capacity significantly affects the treelike structure's stability, security, and economics. This paper utilized experimental verification and numerical modeling to examine the mechanical behavior of cast-steel joints with branches in the treelike structure under various loading conditions. Then, researchers investigated the failure process and mechanism of joints, and the three most common failure modes were outlined. Furthermore, the researchers proposed the bearing capacity calculation formula based on the common failure modes. The results show that the three common failure modes of the cast-steel joints with branches under different loading conditions are the failure in the joint core area under the axial load, the failure in the main pipe compression side under eccentric load, and the failure in the compression side of the single branch pipe root when the single branch pipe is under the uneven load. The suggested empirical calculation method can serve as a reference point for similar engineering practices design.

Keywords: cast-steel joint with branches, numerical simulation, experiment, failure mode, calculation formula

[1]PhD., Eng., Nanyang Institute of Technology, School of Civil Engineering, No. 80 Changjiang Road, 473306 Nanyang, China, e-mail: chenfenghpu@126.com, ORCID: 0000-0003-2399-2906
[2]PhD., Eng., Nanyang Institute of Technology, School of Civil Engineering, No. 80 Changjiang Road, 473306 Nanyang, China, e-mail: sunyun@nyist.edu.cn, ORCID: 0000-0001-8999-6171
[3]B.E, Eng., Nanyang Institute of Technology, School of Civil Engineering, No. 80 Changjiang Road, 473306 Nanyang, China, e-mail: 1204140014@qq.com, ORCID: 0009-0001-2776-2596
[4]MSc., Eng., Nanyang Institute of Technology, School of Civil Engineering, No. 80 Changjiang Road, 473306 Nanyang, China, e-mail: songda@nyist.edu.cn, ORCID: 0009-0008-5616-7607
[4]PhD., Eng., Nanyang Institute of Technology, School of Civil Engineering, No. 80 Changjiang Road, 473306 Nanyang, China, e-mail: ybliu1123@sohu.com, ORCID: 0000-0003-1080-1795

1. Introduction

Large-span space constructions symbolize the nation's building science and technology since they use various new materials and technologies and innovative and prolific designs [1–4]. Joints are typically utilized in critical parts with huge loads and complicated stress, which plays a guiding role in ensuring the safety of the entire large-span space structures. Moreover, joints with simple processing, easy installation, and low cost are also highly advantageous for developing spatial structures. Common space structure joints consist of welded hollow spherical joints, bolted spherical joints, and cast steel joints [5–9]. In recent years, a combination of theory, experiment, and considerable computer analysis has been included in the study methodology for large-span space structures. As construction levels advance, the categorization of large-span space constructions is expanding significantly. The treelike structure based on the bionics concept is increasingly utilized in long-span spatial constructions due to its novel and attractive structural configuration, excellent bearing performance, and remarkable capacity for comprehensive covering [10, 11]. In order to provide a seamless transition and weight transfer between the main pipe and all branch pipes, the cast-steel joint with branches is often employed as a crucial component of the treelike structure [12, 13].

On the one hand, the welding portion between the joint and components can be moved away from the joint's communal area. Alternatively, it can minimize building construction difficulties and enhance safety. However, each level branch of the treelike structure is only connected by a single joint. The failure of the joint will inevitably result in the collapse of the superstructure. Consequently, it is crucial to investigate the bearing capability of cast steel joints with branches. Sun [14] conducted a theoretical study of the cast-steel joint with three branches. Utilizing SolidWorks and ANSYS software, they successfully modeled and analyzed the mechanical characteristics of the joint under axial load. Tan [15] examined the joint construction technology of the treelike structure, analyzing and discussing the selection, manufacturing, installation, and other joint-related technical issues. The bending bearing capacity of the cast-steel joint with four branches was studied by Wu [16, 17]. They comprehensively analyzed the factors affecting the bearing capacity of the joint and provided a formula for calculating the bending bearing capacity of a cast-steel joint with four branches. Du [18] studied the mechanical performance of cast steel joints with branches subjected to eccentric loads and described this type of joint's contributing elements and failure processes. However, these studies focus solely on the theoretical analysis of cast steel joints with branches, and their relevant experimental validation is insufficient and lacks a systematic approach. Consequently, additional research is required to master the mechanical properties of cast steel joints with branches. The number of optimization design approaches for cast steel joints with branches is progressively growing to enhance design efficacy and mechanical performance rationale. Wang [19] proposed the topology optimization technique for the cast steel joint with branches, which is effective and practical for determining the optimal joint form. The joint for topology optimization was made using 3D printing techniques, so resolving the primary issue that the complicated shape formed by topology optimization is difficult to construct using conventional technology. Wang [20] developed an integrated technique based on generative design and additive manufacturing to obtain an optimal cast steel joint that can improve joint production's manufacturing technology precision. Subsequently, they proposed that generative design and powder bed fusion on cast steel joints with branches enhance intelligent construction optimization and feasibility [21].

These studies focus on the design approaches and production procedures for cast steel joints with branches that transcend conventional design. The objective remains to encourage using cast steel joints with branches in engineering practice. Nevertheless, these methodologies are viable as investigation avenues, but there is still a considerable gap in the application of engineering practice. Therefore, to improve the engineering application of cast steel joints with branches, this paper studies the joint's mechanical characteristics under different loading conditions through experimental research and numerical simulation. The joint's stress distribution and failure mechanism are evaluated, and the joint's primary failure modes are outlined. Then, practical formulas for bearing capacity with various failure causes were devised.

2. Experimental study

2.1. Material property

The cast-steel joint with branches is composed of a concurrent intersection between a main pipe and multiple branch pipes. The geometric parameters that affect the mechanical performance of the joint are the angle (θ) between the main pipe and branch pipes, the main pipe length (L), the primary pipe diameter (D), the central pipe wall thickness (T), the branch pipe length (l), the branch pipe diameter (d), the branch pipe wall thickness (t), the chamfer radius (R_1) between the main pipe and the branch pipes, the outside chamfer radius (R_2) between the branch pipe and the branch pipe, and the inside chamfer radius (R_3) among the branch pipes. Figure 1a shows the geometrical features of the joint. Tensile specimens were conducted first to obtain the material properties of the studied joint members. The tensile tests, which adhere to the Chinese code GB/T228.1-2021, were conducted using an INSTRON 1342 dynamic and static material testing machine [22]. The testing specimen is depicted in Figure 1b. The stress–strain (σ–ε) relationship curve for the specimen in the material property test is plotted in Figure. 1c. The specimen's material property testing results are f_y = 265 MPa, E = $2.11 \cdot 10^5$ MPa, and f_u = 394 MPa, respectively. The ultimate strain is 13.68%, the fracture strain is 25.9%, and the ultimate-to-yield strength ratio is 1.49. Which meet the standards of Q235 grade steel as specified in code GB50017-2017 [23].

(a) (b) (c)

Fig. 1. Joint: a) Geometrical features, b) testing specimen, c) stress-strain relationship curve

2.2. Experimental program

Two cast steel joints with branch members were selected for the experiment, one for the axial compression and the other for the eccentric compression. Experiments were conducted using electro-hydraulic servo pressure testing equipment manufactured by China's Jinan testing machine manufacturer. The machine is digitally controlled with a load capacity of 1000 t, which can handle the maximum load requirements. Figure 2 depicts the loading scheme diagram.

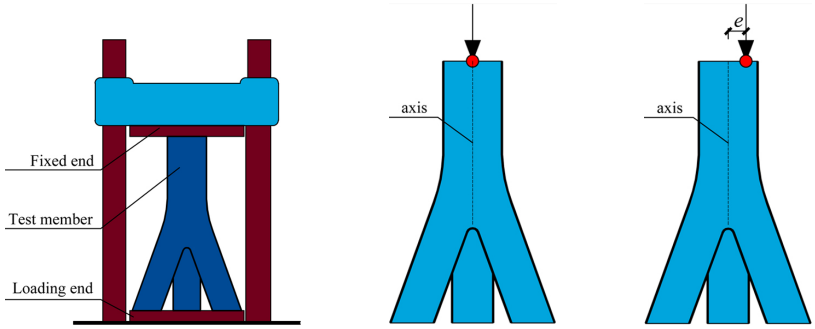

Fig. 2. Loading device schematic diagram: a) device, b) axial load, c) eccentric load

The experiment device schematic diagram is shown in Figure 2a. The loader is a hydraulic jack positioned at the bottom end of the member, while a height-adjustable beam at the top end restricts vertical movement. For the axial compression experiment, the load should be along the axis, while in the eccentric compression experiment, the load was applied along the axis with an eccentric, as shown in Figure 2b and Figure 2c.

2.3. Axial compression experiment

A full-scale experiment was carried out to understand the mechanical behavior of the cast steel joint with branches under axial load. The joint member was produced by Xinxiang Tengfei Factory in China and transported to the structural laboratory for test. Figure 3a depicts the test member and loading apparatus under axial load. The formal loading consisted of five steps, with each stage applying 1000 kN. The loading rate was 10 kN/s. The experiment loader measured the member's vertical displacement during the test, while strain gages and strain rosettes measured the member's stress variation. The placements of the measurement points were separated into three areas: the main pipe upper part, the main pipe lower part, and the joint core area (the intersection of the main pipe and the branch pipe). The position of the measurement point is symmetrical, with three copies throughout the joint's circumference. Figure 3b depicts a frontal view of the measurement locations at the joint. Strain gauges were located at the main pipe's upper and lower parts, where the stress distribution was straightforward. The strain rosette was located near the joint core area where the principal stress direction is unclear, and the stress distribution is complicated.

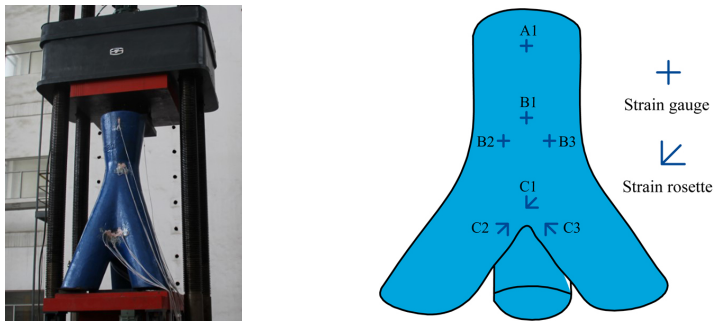

(a) (b)

Fig. 3. Axial compression experiment: a) member and loading device, b) measuring point

The strain gauge model is 120-5AA, the sensitivity coefficient is 2.0 ±1% mV/V, the base dimension is 6.9 × 3.9 mm, the grid size is 2.0 × 1.0 mm, the strain limit value is 20000 um/m and the applicable temperature range is –20~80°C. The strain rosette model is 120-2CA-D150, the sensitivity coefficient is 2.0 ±1% mV/V, the base dimension is 9.0 × 9.0 mm, the grid size is 3.0 × 2.3 mm, the strain limit value is 20000 um/m and the applicable temperature range is –20 ~80°C. The placements of the measurement points were separated into three areas: the main pipe upper part, the main pipe lower part, and the joint core area (the intersection of the main pipe and the branch pipe). The position of the measurement point is symmetrical, with three copies throughout the joint's circumference. When the following phenomenon happens during the loading process, it means that a plastic zone is forming in the member, which is approaching its ultimate bearing capacity state: (a) Excessive strain variation at the measurement locations; (b) The test member undergoes obvious deformation visible to the naked eye; (c) The loading machine displays unloading. During this process, the testing machine's maximum load reading is the ultimate bearing capacity of the member. After each load level was applied, strain data were collected and recorded using the strain box DH3815N. The axial compression experiment results are shown in Figure 4.

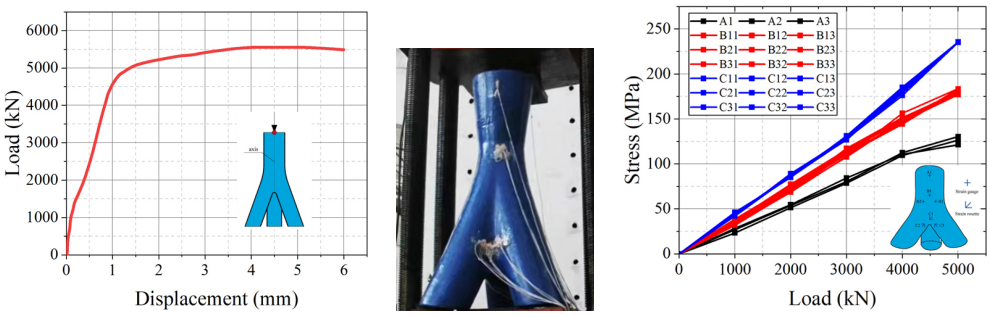

(a) (b) (c)

Fig. 4. Axial compression results: a) relationship curve, b) deformation, c) stress distribution

From figure 4a, it can be seen that the slope of the load-displacement curve grows linearly in the initial stage. The slope exhibits nonlinear oscillations as the load increases, primarily attributable to the loose contact between the member and the loading mechanism. When the load approaches its ultimate carrying capacity, the load-displacement curve looks nonlinear, indicating that the joint has entered the elastic-plastic state. Moreover, the maximum load during the entire loading process is 5584 kN. figure 4b shows the actual deformation of the member. The core area intersection between the member's main pipe and branch pipes is deformed, suggesting that this zone is the most hazardous for the joint under axial force. Figure 4c shows the load-stress relationship curves at each measuring point of the joint under axial load. It may be deduced that the measurement points are essentially symmetrically organized throughout the circumference of the joint axis and that the stress levels of these measuring locations are essentially the same, suggesting that the load is aligned along the axis with little eccentricity. The stress at each measurement location exhibits a linear relationship with load values ranging from 1000 kN to 4000 kN. when the load reaches 5000 kN, the minimum stress is 121.4 MPa at the main pipe, and the maximum is 235.7 MPa at the joint core area. it indicates that the stress at the lower and upper of the main pipe are relatively small, while the stress at the core area is relatively high.

2.4. Eccentric compression experiment

On the 1000 t electro-hydraulic servo pressure testing equipment, a full-scale model experiment for a cast steel joint with branches under eccentric compression was also completed. The experiment's apparatus, loading scheme, and test data collection system are identical to those of the axial compression experiment. Figure 5a shows the joint and loading device for the eccentric experiment. During the experiment, the experiment loader recorded the member's vertical displacement, strain gages, and strain rosettes recorded the member's stress variation. Along the circumferential direction, the measurement point layouts were separated into four regions: the joint main pipe upper part, the main pipe lower part, the joint core area, and the branch pipe end part. The strain gauges are arranged at the main pipe upper (A1-A6) and lower (B1-B6). The strain rosettes are arranged at the joint core area (C2, C4, and C6) and the branch pipe end part (C1, C3, and C5). Figure 5b shows a frontal view of the measurement locations at the joint. The DH3815N strain box was also used to measure and collect strain data.

The eccentric compression experiment results are shown in Figure 6. In the initial loading stage, the load-displacement curve tends to be linear, and the member is subject to the elastic stage. As the load approaches bearing capacity, the curve appears nonlinear, indicating that the joint has entered the elastic-plastic state. Moreover, the maximum load during the entire loading process is 4437 kN. Figure 6b shows the actual deformation of the member. It can be observed that the compression side of the main pipe has a noticeable deformation, indicate that this zone is the most hazardous for the memeber under eccentric load. Figure 6c shows the stress at each measuring point of the joint under eccentric load. The maximum stress at the main pipe upper part is 235.2 MPa, which occurs on the compressed side and the tensile side is 108.6 MPa, while the joint core area tensile side is 185.2 MPa and the stress on the compressive side is 132.6 MPa. This shows a significant difference in stress levels between the compressive

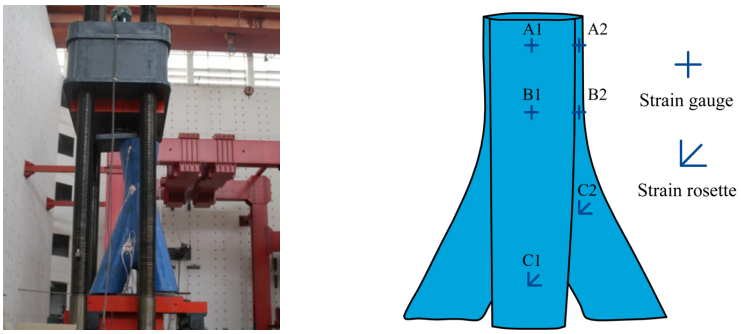

Fig. 5. Eccentric compression experiment: a) member and loading device, b) measuring point

and tensile sides, and the impact of the bending moment is notable. The maximum stress of the branch pipe end part is 138.2 MPa, located on the compressive side, and the minimum stress is 132.5 MPa on the tensile side. The stress change magnitude is relatively small, indicating that the bending moment has a negligible impact on the stress distribution of the branch pipe. The branch pipes' stress level is relatively small, suggesting the branch pipes' wall thickness can be appropriately reduced while the bearing capacity of the joints is ensured in engineering.

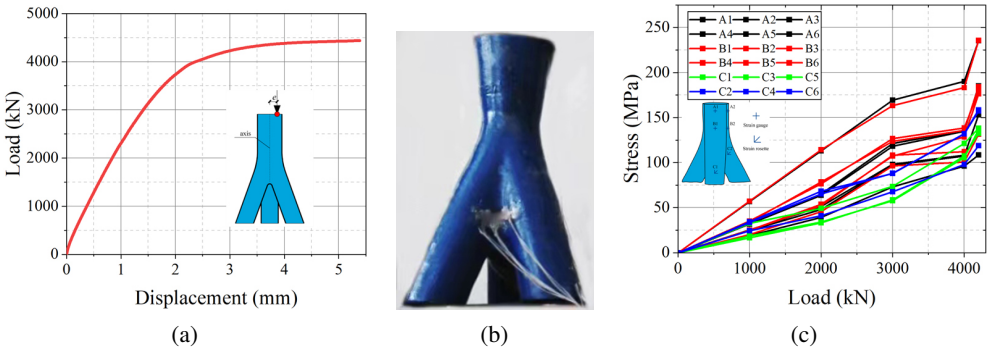

Fig. 6. Eccentric compression results: a) curve, b) deformation, c) stress distribution

3. Finite element analysis

3.1. Establish model

Using the existing finite element software to construct a joint model makes it challenging to achieve the seamless transition of the joints. This paper uses SolidWorks, a 3D modeling software widely used in mechanical engineering, to realize the modeling of complex geometry

structures. It can construct the model of cast-steel joint with branches with a smooth transition and realize the upper-end face of branch pipes along the horizontal direction (Figure 7a) or vertical to the branch pipes axis to be compatible with the actual project (Figure 7b). The established joint model was imported into the finite element software ANSYS for analysis. The model material of the joint is made of ZG20SiMn steel. The elastic modulus of the material (E) is $2.0 \cdot 10^5$ N/mm^2, the yield strength (f_y) is 235 MPa, and the Poisson's ratio (μ) is 0.3. The researchers chose the ideal elastic-plastic model to simulate the constitutive behavior of the material [24–26]. The Von Mises stress yield criterion and associated flow rule were used for the elastic-plastic analysis. The whole process response of the load displacement about the joint was iteratively tracked by using the arc length method. After comparison, the researchers chose the three-dimensional solid element Solid65 from the ANSYS element type library. The element type has a quadratic displacement and is suitable for irregular grid division [27–30]. Figure 7c shows the joint finite element mesh.

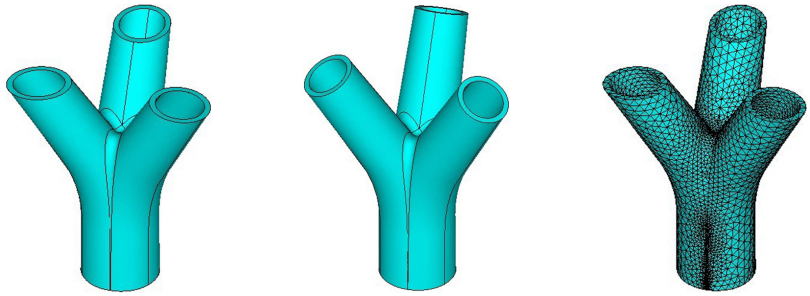

(a) (b) (c)

Fig. 7. Joint Models: a) horizontal, b) vertical branch pipes axis, c) finite element mesh

3.2. Axial compression analysis

The finite element analysis of the axial compression experiment joint was carried out. The boundary conditions are simplified as the main pipe end was fixed, and the branch pipes were free. The load was applied to the branch pipe end in a manner of surface pressure. Figure 8a shows the joint stress contour to enter the plastic stage. It indicates that although the stress level of the main pipe and the branch pipe is lower, the yield strength of the joint core area reaches first, and the core area is the weak part of the joint. Figure 8b shows the stress contour of the joint reaching its ultimate bearing capacity. It indicates that, with the increasing load, the plastic zone expands further along the joint core area. Finally, the joint loses the ability to continue carrying loads due to forming a plastic hinge in the core area. In the process, the stress level of the main pipe and branch pipes has significantly increased, but it is far from reaching the yield strength of the joint. Therefore, the joint failure mode under the axial load is the destruction at the core area intersection between the main pipe and branch pipes. The finite element results were compared with the experimental results to verify the accuracy of the finite element analysis. According to the arrangement position of the measuring point,

researchers extracted the representative points A2 (the main pipe upper part), B22 (the main pipe lower part), and C22 (the joint core area) stress values of finite element calculation results and experiment results. Figure 8c shows the comparison results. The finite element results (FE) agree with the experiment results (EX), which show that the finite element method is correct and the procedure is feasible. From the stress variation characteristics of points A2, B22, and C22, the stress value at the core area is more prominent, while the stress value at the main pipe and branch pipes is smaller under the same load. Moreover, the stress distribution rules of the test results are consistent with the finite element calculation results.

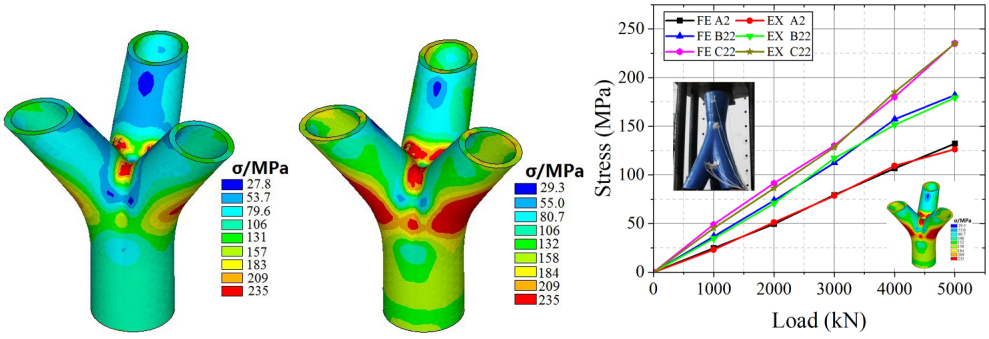

Fig. 8. Axial analysis: a) entering plasticity, b) reaching bearing capacity, c) comparison results

3.3. Eccentric compression analysis

When the finite element analysis was carried out on the eccentric compression joint, the boundary conditions were simplified as the branch pipes end part was fixed, the main pipe end part was free, and the eccentric load was applied to the main pipe end with a certain eccentricity. Figure 9a shows the stress contour of the eccentric compression joint entering plasticity, and only the main pipe's compression side reaches the joint's yield strength, showing that the main pipe's compression side is the joint's weak part. Figure 9b shows the stress contour of the joint reaching its ultimate bearing capacity, indicating that the plastic zone on the compression side of the main pipe has expanded further along the circumferential direction of the main pipe. When the main pipe's compression side reaches the joint's ultimate bearing capacity, it will be destroyed. In the process, the stress level at the tensile side of the main pipe and the other parts of the joint is low and far from reaching the yield strength. Therefore, the joint failure mode under the eccentric load is the destruction at the end of the compression side of the main pipe. Stress values of finite element calculation results and experiment results of the points at the compression side (A1, B1, and C1) and tensile side (A4, B4, and C4) under different load stages were extracted and compared, as shown in Figure 9c. As can be seen that the test results and finite element calculation results are in good agreement. The compression side of the main pipe reaches the yield strength at first which indicates the main pipe's compression side is the joint's weak part.

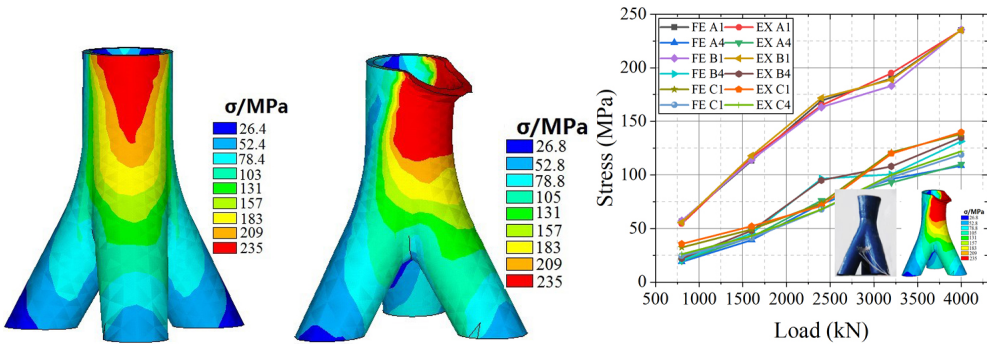

(a) (b) (c)

Fig. 9. Eccentric analysis: a) entering plasticity, b) bearing capacity, c) comparison results

3.4. Branch pipe under the uneven load analysis

When the treelike structure is subjected to uneven load, massive internal forces may be generated in one of the branch pipes. Therefore, researchers carried out the finite element analysis of the single branch pipe under uneven load. The joint's calculation model fixed the main pipe's end, and the branch pipes were free. The load was applied to the upper end of one branch pipe. Figure 10a shows the stress contour of the joint entering plasticity. As can be seen that the compression side at the root of the branch pipe initially appears to bend while the stress level at other parts is lower, which indicates that the root of the compression branch is the weak part of the joint. Figure 10b shows the stress contour of the joint reaching its ultimate bearing capacity. As can be seen that the plastic zone of the joint expanded further until the intersection between the main pipe and the branch pipe entered the plastic zone ultimately. Finally, the joint was destroyed for the plastic hinge formed in the root of the loaded branch pipe.

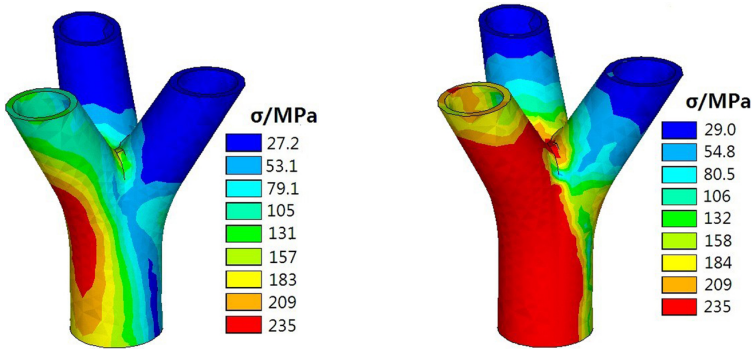

(a) (b)

Fig. 10. Uneven load analysis: a) entering plasticity, b) reaching bearing capacity

4. Design method

4.1. Calculation formula establishment for axial compression

A comprehensive analysis of the existing norms and the study's results on the different joint calculation formulas shows a particular function between the bearing capacity and the geometric parameters, material strength. The bearing capacity formulas [31–34] of the welded tubular T-joints, the steel tubular XK-joints, and the multi-planar KX- and KT-joints under axial loads are all expressed as Eq. (4.1). The cast steel joint with branches has the same characteristics, and the same formula form can express the bearing capacity calculation formula.

$$F_u = KT^2 f_y \tag{4.1}$$

where F_u is the bearing capacity of the joint; K is a parameter that contains the geometric parameters such as θ, γ, β, and R_3 of the joint; T is the pipe wall thickness; and f_y is the material yield strength of the joint.

In Eq. (4.1) expression of K is the research focus for different types of joints. Since K is a comprehensive index reflecting the influence of various geometric parameters on the joint bearing capacity, it is no longer a single study of the relationship between K and F_u but a multiple of the relationship between each parameter and K. The parameters θ, γ, β, and R_3 significantly influence the joint bearing capacity. However, the parameters L, R_1, and R_2 of the joint have little influence on the joint bearing capacity, so these three parameters are ignored during the analysis of comprehensive index K.

The functional relationship between the K_θ and θ was analyzed. The relationship between the sine value of θ and K_θ in Eq. (4.2).

$$K_\theta = 0.60022 - 2.5311 \sin\theta + 6.59681 \sin^2\theta - 5.07388 \sin^3\theta \tag{4.2}$$

The relationship between γ and K_γ could be expressed as the power function in Eq. (4.3).

$$K_\gamma = 4.3725\gamma^{0.66242} \tag{4.3}$$

The linear relationship between the β and K_β could express as Eq. (4.4).

$$K_\beta = 1 + 0.58856\beta \tag{4.4}$$

The regression analysis is conducted between R_3 and K_{R_3}. According to the principle of dimensional analysis, it is required that the item of R_3 contained in the formula is dimensionless. Eq. (4.5) defined a dimensionless chamfer coefficient ρ to consider the influence of R_3.

$$\rho = \frac{R_3}{\sqrt{dt}} \tag{4.5}$$

where d is the outer diameter of the branch pipe; t is the wall thickness of the branch pipe.

The finite element model shows that the joint ultimate bearing capacity is minimal when R_3 exceeds or is equal to 100 mm. So R_3 is limited to less than or equal to 100 mm on the ultimate

bearing capacity calculation formula for the cast-steel joint with three branches. Through regression analysis, the Chamfer coefficient ρ and K_{R_3} relationship follows a linear relation that could express as Eq. (4.6).

$$K_{R_3} = 1 + 0.33738\frac{R_3}{\sqrt{dt}} \tag{4.6}$$

Because these four parameters are independent, the joint bearing capacity formula can be obtained by multiplying them, following the method of establishing the bearing capacity on joints in the existing standards, expressed as Eq. (4.7).

$$F = 4.37251\gamma^{0.66242}\left(1 + 0.58856\beta\right)\left(1 + 0.33738\frac{R_3}{dt}\right)\cdot \cdot \left(0.60022 - 2.5311\sin\theta + 6.59681\sin^2\theta - 5.07388\sin^3\theta\right) f_y T^2 \tag{4.7}$$

4.2. Calculation formula establishment for eccentric compression

The formula of the bearing capacity of joints under eccentric load can be simplified based on the failure mode of the joint. After a comprehensive analysis of the experiment results and the finite element analysis results, the cross-section of the main pipe can be used in the calculation model for the bearing capacity of the joint. Figure 11 shows the simplified model. M is the moment, N is the axial load, and e is the eccentricity.

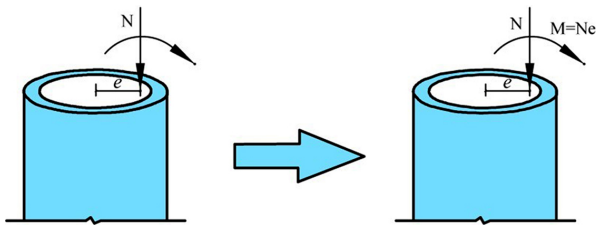

Fig. 11. Simplified calculation model for eccentric compression

Equation (4.8) shows the formula of cast steel joints with three branches under eccentric compression load.

$$\sigma = \frac{N}{A} + \frac{M}{W} \leq [\sigma] \tag{4.8}$$

Where A is the cross-sectional area of the main pipe, W is the section modulus in bending of the main pipe, and $[\sigma]$ is allowable stress.

We can obtain Eq. (4.9) by substituting all the geometric parameters of the joint into the Eq. (4.8).

$$\sigma = \frac{N}{\pi\left(DT - T^2\right)} + \frac{32M}{\pi D^3\left[1 - \left(1 - \frac{2T}{D}\right)^4\right]} \leq [\sigma] \tag{4.9}$$

where D is the outside diameter of the main pipe, and T is the wall thickness of the main pipe.

The bending moment the Eq. (4.10) can obtain M.

$$M = N \cdot e \tag{4.10}$$

In the end, researchers obtained the formula of the ultimate bearing capacity of the cast steel joint with three branches under eccentric load, as shown in Eq. (4.11).

$$N = \frac{\pi [\sigma] D^3 \left(DT - T^2\right) \left[1 - \left(1 - \frac{2T}{D}\right)^4\right]}{32e \left(DT - T^2\right) + D^3 \left[1 - \left(1 - \frac{2T}{D}\right)^4\right]} \tag{4.11}$$

4.3. Calculation formula establishment for branch pipe under uneven load

The bearing capacity formula of the branch pipe under the uneven load can be simplified based on the failure mode of the joint. Figure 12 shows the simplified model of the root of a branch pipe. M is the bending moment, N is the bearing capacity, and e is the eccentricity.

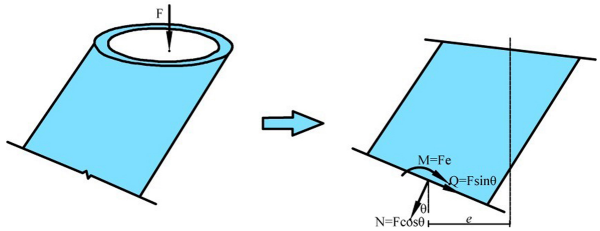

Fig. 12. Simplified calculation model for branch pipe under the uneven load

Equation (4.12) shows the formula of the cast-steel joint with three branches of the single branch pipe under uneven load.

$$\sigma = \sqrt{(\sigma_N + \sigma_w)^2 + 3\tau^2} \leq \sigma] \tag{4.12}$$

where $[\sigma]$ is the allowable stress, σ is the equivalent stress of the joint, σ_N is the stress caused by the axial force, σ_W is the stress caused by the bending moment, and τ is the stress caused by the shear force.

Equation (4.13) shows the stress caused by the axial force.

$$\sigma_N = \frac{N}{A} = \frac{F \cos\theta}{\pi t (d - t)} \tag{4.13}$$

where A is the sectional area of the branch pipe, N is the axial force along the branch pipe section, d is the outside diameter of the branch pipe, t is the wall thickness of the branch pipe, θ is the angle between the main pipe and branch pipe.

Equation (4.14) shows the stress caused by the bending moment.

$$\sigma_w = \frac{M}{W} = \frac{Fe}{W} = \frac{4dFe}{\pi t\,(d-t)\left(d^2+2t^2-dt\right)} \tag{4.14}$$

Equation (4.15) shows the stress caused by the shear force.

$$\tau = \frac{Q}{A} = \frac{F\sin\theta}{\pi t\,(d-t)} \tag{4.15}$$

Q is the shear force.

Finally, researchers obtained the ultimate bearing capacity formula of the single branch pipe under uneven load, as shown in Eq. (4.16).

$$F = \sqrt{\frac{\pi^2 t^2 [\sigma]^2 (d-t)^2 \left(d+2t^2-2dt\right)^2}{\left(d^2+2t^2-2dt\right)\left[\begin{array}{l}\left(d^2+2t^2-2dt\right)+2\sin^2\theta\cdot \\ \cdot\left(d^2+2t^2-2dt\right)+8de\cos\theta\end{array}\right]+16d^2e^2}} \tag{4.16}$$

The calculation formula can be simplified as the Eq. (4.17).

$$F = \sqrt{\frac{\pi^2 t^2 [\sigma]^2 X^2 Y^2}{X(X+2\sin^2\theta X+8de\cos\theta)+16d^2e^2}} \tag{4.17}$$

where, $X = d^2 + 2t^2 - 2dt$ and $Y = d - t$.

5. Conclusions

1. There are three failure modes of the cast-steel joints with branches under different loading conditions: the failure in the core area of the joint under the axial compression load, the failure in the main pipe compression side under eccentric load, and the failure at the compression side of the single branch pipe root when the single branch pipe is under the compression load.
2. The bearing capacity of the joint with bending moment in its internal forces is lower than others. So the bending moment significantly influences the ultimate bearing capacity of the joint. In the joint design, the corresponding staff should reduce the bending moment as far as possible to ensure it mainly bears the axial load.
3. The fillet radius at the intersection between pipe and pipe significantly influences the bearing capacity of the joint. The appropriate fillet radius of the joint can significantly reduce the stress concentration and delay the yield process.
4. The formulas for calculating the bearing capacity based on the different failure modes of the cast steel joint with branches are consistent with the existing formulas in building codes, which can provide a reference for the related engineering design.
5. The branch pipes' stress level is relatively small, suggesting the branch pipes' wall thickness can be appropriately reduced while the bearing capacity of the joints is ensured in engineering.

Acknowledgements

This research was supported by the Nanyang Institute of Technology Ph.D. Research Initiation Fund Project (Grant No. NGBJ-2023-34), Nanyang Institute of Technology Student Research Fund Project and the Science and Technology Plan Project of Nanyang (Grant No. KJGG033).

References

[1] L. Yaozhi and Z. Jingyu, "Research status and future prospects of space structure health monitoring", *Journal of Building Structures*, vol. 43, no. 10, pp. 16–28, 2022, doi: 10.14006/j.jzjgxb.2022.0070.

[2] L. You, L. Yao, X. Li, G. Jia, and G. Lv, "Numerical simulation and casting process optimization of cast steel node", *The International Journal of Advanced Manufacturing Technology*, vol. 126, pp. 5215–5225, 2023, doi: 10.1007/s00170-023-11460-8.

[3] Z. Shu, B. Ning, J. Chen, Z. Li, M. He, J. Luo, and H. Dong, "Reinforced moment-resisting glulam bolted connection with coupled long steel rod with screwheads for modern timber frame structures", *Earthquake Engineering & Structural Dynamics*, vol. 52, no. 4, pp. 845–864, 2023, doi: 10.1002/eqe.3789.

[4] L. Tian, J. Hao, J. Wei, and J. Zheng, "Integral lifting simulation of long-span spatial steel structures during construction", *Automation in Construction*, vol. 70, pp. 156–166, 2016, doi: 10.1016/j.autcon.2016.06.015.

[5] Y. Yin, X. Che, Z. Li, J. Li, and Q. Han, "Ductile fracture analysis of welded hollow spherical joints subjecting axial forces with micromechanical fracture models", *International Journal of Steel Structures*, vol. 19, pp. 2010–2023, 2019, doi: 10.1007/s13296-019-00261-z.

[6] X. Xu, T. Shu, J. Zheng, and Y. Luo, "Experimental and numerical study on compressive behavior of welded hollow spherical joints with external stiffeners", *Journal of Constructional Steel Research*, vol. 188, art. no. 107034, 2022, doi: 10.1016/j.jcsr.2021.107034.

[7] Z. Wei, H. Jin, X. Pei, and L. Wang, "A simplified approach to estimate the fatigue life of full-scale welded cast steel thin-walled tubular structures", *Thin-Walled Structures*, vol. 160, art. no. 107348, 2021, doi: 10.1016/j.tws.2020.107348.

[8] B. Ding, Y. Zhao, Z. Huang, L. Cai, and N. Wang, "Tensile bearing capacity for bolted spherical joints with different screwing depths of high-strength bolts", *Engineering Structures*, vol. 225, art. no. 111255, 2020, doi: 10.1016/j.engstruct.2020.111255.

[9] H. Yuan, H. Liu, X. Ren, and X. Zhang, D. Ai, Y. Luo, "The bearing performance of the bolt-sphere joints with stochastic pitting corrosion damage", *Journal of Constructional Steel Research*, vol. 160, pp. 359–373, 2019, doi: 10.1016/j.jcsr.2019.05.032.

[10] J. Hunt, W. Haase, and W. Sobek, "A design tool for spatial tree structures", *Journal of the International Association for Shell and Spatial Structures*, vol. 50, no. 1, pp. 3–10, 2009.

[11] Y.C. Shi, L.W. Tong, "Current application and future outlook of mechanic bionics in buildings of steel structure", *Journal of Structural Engineers*, vol. 23, no. 2, pp. 5–8, 2007.

[12] G. Sun, R. Yue, and Z. Chen, S. Xue, "Numerical and experimental research of the design method of plate-insert welded tubular joint", *Journal of Structural Engineering*, vol. 147, no. 9, art. no. 4021129, 2021, doi: 10.1061/(ASCE)ST.1943-541X.0003102.

[13] S. Qu, X. Wu, and Q. Sun, "Experimental study and theoretical analysis on the ultimate strength of high-strength-steel tubular K-Joints", *Thin-Walled Structures*, vol. 123, pp. 244–254, 2018, doi: 10.1016/j.tws.2017.11.014.

[14] Z.F. Sun, "The theoretical study of cast steel branch joints in tree structures", M.A. thesis, Henan University, China, 2014.

[15] Z.Y. Tan, "Dendriform structure construction technology and application", M.A. thesis, Chongqing University, China, 2002.

[16] W.H. Wu and W.F. Du, "Loaded analysis of spatial cast-steel joint with four branches in treelike structure", *Journal of Henan University (Natural Science)*, vol. 44, no. 6, pp. 738–742, 2011.

[17] W.F. Du, Z.F. Sun, B.Q. Gao, and S.L. Dong, "Finite element analysis of a cast-steel joint with three branches in treelike structure", *Journal of Building Structures*, vol. 35, no. S1, pp. 89–93, 2014, doi: 10.14006/j.jzjgxb.2014.s1.014.

[18] W. Du, Y. Sun, and M. Yang, "Bearing capacity of the cast-steel joint with branches under eccentric load", *Journal of Constructional Steel Research*, vol. 135, pp. 285–291, 2017, doi: 10.1016/j.jcsr.2017.04.005.

[19] L. Wang, W. Du, P. He, and M. Yang, "Topology optimization and 3D printing of three-branch joints in treelike structures", *Journal of Structural Engineering*, vol. 146, no. 1, art. no. 4019167, 2020, doi: 10.1061/(ASCE)ST.1943-541X.0002454.

[20] H. Wang, W. Du, Y. Zhao, Y. Wang, R. Hao, and M. Yang, "Joints for treelike column structures based on generative design and additive manufacturing", *Journal of Constructional Steel Research*, vol. 184, art. no. 106794, 2021, doi: 10.1016/j.jcsr.2021.106794.

[21] H. Wang, W. Du, Y. Zhao, Y. Wang, and M. Yang, "Optimization and experimental research on treelike joints based on generative design and powder bed fusion", *Engineering Structures*, vol. 278, art. no. 115564, 2023, doi: 10.1016/j.engstruct.2022.115564.

[22] GB/T 228.1:2021 Metallic materials-Tensile testing-Part 1: Method of test at room temperature. China Architecture & Building Press, 2021.

[23] GB50017:2017 Standard for design of steel structures: GB50017-2017. China Architecture & Building Press, 2017.

[24] J. Chen, Q.L. Zhang, and B.Y. Xie, "Research and application of dendritic column in long-span spatial structure", *Journal of Steel Construction*, vol. 3, no. 25, pp. 1–5, 2010.

[25] S.H. Kim, K.I. Cho, J.H. Won, and J.H. Kim, "A study on thermal behavior of curved steel box girder bridges considering solar radiation", *Archives of Civil and Mechanical Engineering*, vol. 9, no. 3, pp. 59–76, 2009, doi: 10.1016/S1644-9665(12)60218-0.

[26] J. Noorzaei, K.H. Bayagoob, W.A. Thanoon, and M.S. Jaafar, "Thermal and stress analysis of Kinta RCC dam", *Engineering Structures*, vol. 28, no. 13, pp. 1795–1802, 2006, doi: 10.1016/j.engstruct.2006.03.027.

[27] E. Hamed, M. Bradford, and R. Gilbert, "Time-dependent and thermal behavior of spherical shallow concrete domes", *Engineering Structures*, vol. 31, no. 9, pp. 1919–1929, 2009, doi: 10.1016/j.engstruct.2009.01.022.

[28] Z. Wei, X. Pei, and H. Jin, "Evaluation of welded cast steel joint fatigue data using structural stress methods", *Journal of Constructional Steel Research*, vol. 186, art. no. 106895, 2021, doi: 10.1016/j.jcsr.2021.106895.

[29] L. Tong, Y. Chen, and Y. Chen, "Cyclic behaviour of beam-to-column joints with cast steel connectors", *Journal of Constructional Steel Research*, vol. 116, pp. 114–130, 2016, doi: 10.1016/j.jcsr.2015.09.005.

[30] L. Wu, X. Li, and H. Deng, "Flexural performance of hybrid fiber reinforced cement-based materials incorporating ceramic wastes", *Archives of Civil Engineering*, vol. 69, no. 3, pp. 491–506, 2023, doi: 10.24425/ace.2023.146093.

[31] CECS235: 2008 Technical specification for application of connections of structural steel casting.

[32] ANSI/AISC 360-05:2005 Specification for Structural Steel Buildings.

[33] EN 1993-1-8 Eurocode 3: Design of steel structures. Part 1.8.

[34] S. Herion, J.C.D. Oliveira, J.A. Packer, C. Christopoulos, and M.G. Gray, "Castings in tubular structures-the state of the art", *Proceedings of Institution of Civil Engineering Structures and Buildings*, vol. 163, no. 6, pp. 403–415, 2010, doi: 10.1680/stbu.2010.163.6.403.

Received: 2023-09-01, Revised: 2023-10-31